Origin of meteoritic stardust unveiled by a revised proton-capture rate of 17 O

Origin of stardust unveiled by the new rate of the ^{17}O(p,α)^{14}N reaction

M. Lugaro[1,2], A. I. Karakas[2,3,4], C. Bruno[5], M. Aliotta[5], L. R. Nittler[6], D. Bemmerer[7], A. Best[8], A. Boeltzig[9], C. Broggini[10], A. Caciolli[11], F. Cavanna[12], G. F. Ciani[9], P. Corvisiero[12], T. Davinson[5], R. Depalo[11], A. Di Leva[8], Z. Elekes[13], F. Ferraro[12], A. Formicola[14], Zs. Fülöp[13], G. Gervino[15], A. Guglielmetti[16], C. Gustavino[17] Gy. Gyürky[13], G. Imbriani[8], M. Junker[14], R. Menegazzo[10], V. Mossa[18], F. Pantaleo[18], D. Piatti[11], P. Prati[12], D. A. Scott[5], E. Somorjai[13], O. Straniero[19], F. Strieder[20,21], T. Szücs[13], M. P. Takács[7], D. Trezzi[16]

[1]*Konkoly Observatory, Research Centre for Astronomy and Earth Sciences, Hungarian Academy of Sciences, H-1121 Budapest, Hungary*

[2]*Monash Centre for Astrophysics (MoCA), Monash University, Clayton VIC 3800, Australia*

[3]*Research School of Astronomy and Astrophysics, Australian National University, Canberra, ACT 2611, Australia*

[4]*Kavli Institute for the Physics and Mathematics of the Universe (WPI), University of Tokyo, Kashiwa, Chiba 277-8583, Japan*

[5]*SUPA, School of Physics and Astronomy, University of Edinburgh, EH9 3FD Edinburgh, United Kingdom*

[6]*Department of Terrestrial Magnetism, Carnegie Institution for Science, Washington, DC 20015, USA*

[7]*Helmholtz-Zentrum Dresden-Rossendorf, Bautzner Landstr. 400, 01328 Dresden, Germany*

[8]*Università di Napoli Federico II and INFN, Sezione di Napoli, 80126 Napoli, Italy*

[9]*Gran Sasso Science Institute, INFN, Viale F. Crispi 7, 67100 L'Aquila, Italy*

[10]*INFN of Padova, Via Marzolo 8, I-35131 Padova, Italy*

[11]*Università degli Studi di Padova and INFN, Sezione di Padova, Via F. Marzolo 8, 35131 Padova, Italy*

[12]*Università degli Studi di Genova and INFN, Sezione di Genova, Via Dodecaneso 33, 16146 Genova, Italy*

[13]*Institute for Nuclear Research (MTA ATOMKI), PO Box 51, HU-4001 Debrecen, Hungary*

[14]*INFN, Laboratori Nazionali del Gran Sasso (LNGS), 67100 Assergi, Italy*

[15]*Università degli Studi di Torino and INFN, Sezione di Torino, Via P. Giuria 1, 10125 Torino, Italy*

[16]*Università degli Studi di Milano and INFN, Sezione di Milano, Via G. Celoria 16, 20133 Milano, Italy*

[17]*INFN, Sezione di Roma La Sapienza, Piazzale A. Moro 2, 00185 Roma, Italy*

[18]*Università degli Studi di Bari and INFN, Sezione di Bari, 70125 Bari, Italy*

[19]*Osservatorio Astronomico di Collurania, Teramo, and INFN, Sezione di Napoli, 80126 Napoli, Italy*

[20]*Institut fr Experimentalphysik III, Ruhr-Universitt Bochum, 44780 Bochum, Germany*

[21]*Present address: South Dakota School of Mines, 501 E. Saint Joseph St., SD 57701 USA*

Stardust grains recovered from meteorites provide high-precision snapshots of the isotopic composition of the environment in which they formed. Establishing their stellar sites of origin, however, often proves difficult. Asymptotic giant branch (AGB) stars of initial mass

greater than 4 solar masses produce substantial amounts of dust during their evolution and are predicted to be the site of origin of a large fraction of meteoritic stardust[1,2]. Yet, no grains have been found to date whose origin can be attributed to these massive AGB stars, potentially highlighting gaps in our understanding of the lifecycle of stars and dust in the Galaxy. Here we show that using the new, increased rate of the ^{17}O(p,α)^{14}N reaction[3] based on a recent underground experiment, we can account for a population of stardust grains that show the ^{17}O/^{16}O ratios expected from H burning at temperatures of 60–80 million K characteristic of massive AGB stars. This result provides the first direct evidence that these stars contributed to the dust inventory from which the Solar System formed.

Stardust grains found in meteorites represent the very small fraction of presolar dust that survived destruction in the protosolar nebula. They condensed in the atmospheres of evolved stars and in supernova ejecta and were preserved inside meteorites[4]. Their isotopic compositions are measured with high precision (few percent uncertainties) via mass spectrometry and represent a direct record of their site of formation, providing us with deep insights into stellar physics and the origin of elements and of dust in the Galaxy. Identified stardust includes both carbon-rich (diamonds, graphite, silicon carbide) and oxygen-rich (corundum, spinel, hibonite, silicate) grains, with the former condensing from gas with C>O, and the latter from gas with C<O. Here we focus on oxide and silicate grains, which are classified into different groups mostly based on their O isotopic compositions[5]. Group I grains make up the majority of oxide and silicate grains and show excesses in ^{17}O corresponding to the signature of the first dredge-up in red giant stars of initial mass roughly 1–3 $\mathrm{M}_{\odot}$. Their origin is generally well understood and attributed to the O-rich phases of

the subsequent asymptotic giant branch (AGB), when large amounts of dust condense in the cool, expanding stellar envelopes[1]. Group II grains represent roughly 15% of all presolar oxide grains. Like Group I grains, they also display excesses in ^{17}O but are highly depleted in ^{18}O, with ^{18}O/^{16}O ratios down by two orders of magnitude relative to solar. The initial ratio of the radioactive ^{26}Al (half life, $T_{1/2} = 0.7$ Myr) to ^{27}Al is also inferred from ^{26}Mg excesses and it is as high as 0.1 in Group II grains, almost an order of magnitude higher than in Group I grains on average. While this composition is the indisputable signature of H burning activating proton captures on the O isotopes and on ^{26}Mg (the ^{26}Mg(p,γ)^{26}Al reaction), hypotheses on the site of formation of Group II grains are still tentative.

Hydrogen burning affects the surface composition of massive ($> 4\ M_{\odot}$) AGB stars when the base of the convective envelope becomes hot enough for proton-capture nucleosynthesis to occur[6] ("hot bottom burning", HBB, Figure 1). These are the brightest AGB stars, and the fact that they mostly show C/O$<$1 is attributed to the operation of the CN cycle, which converts C into N[7], in contrast to their less bright counterparts, which mostly show C/O$>$1 as a result of the dredge-up of He-burning material rich in C. Characteristic temperatures of HBB are higher than $\sim\ 60$ MK and, thanks to the fast convective turn-over time (≈ 1 yr), the composition of the whole envelope is quickly transmuted into the H-burning equilibrium yields produced at the base of the envelope. Massive AGB stars are observed to generate significant amounts of dust and are expected to have contributed almost half of the O-rich dust of AGB origin in the Solar System[1,2]. However, no stardust grains have been found to show the signature of HBB because the expected ^{17}O/^{16}O ratios calculated with available reaction rates[8] are roughly twice as high as those observed in the Group

II grains[9–11].

The currently, alternative suggestion for the origin of Group II grains is that they formed in AGB stars of low mass ($<$1.5–1.7 $\mathrm{M}_{\odot}$) that do not dredge-up enough C to become C-rich but experience instead extra mixing below the bottom of the convective envelope ("cool bottom processing", CBP[12,13], Figure 1). In this scenario, material from the bottom of the convective envelope penetrates the thin radiative region located between the base of the convective envelope and the top of the H-burning shell where temperature and density increase steeply with mass depth and proton captures can occur (Figure 1). While scenarios have been formulated to explain the physical process driving this extra mixing[14] the current modelling of the CBP is parametric: both the rate of the extra mixing and the depth reached are treated as a free parameters, with the depth set in order to reach temperatures in the range 40–55 MK.

Whichever scenario we consider, the equilibrium ^{17}O/^{16}O ratio produced by H burning in AGB stars is determined by the competition between the processes that produce and destroy ^{17}O. Specifically, it depends on the ratio between the rate of the ^{16}O(p,γ)^{17}F reaction, which produces ^{17}O following the beta decay of ^{17}F ($\mathrm{T}_{1/2} = 64$ s) and the rate of the ^{17}O(p,α)^{14}N reaction, which destroys ^{17}O. (Note that the ^{17}O(p,γ)^{18}F is comparatively negligible at all temperatures considered here). The former is known to within 7%[8,11]; the latter has recently been determined[3] from a direct measurement of the strength of the 70 keV resonance that dominates the ^{17}O(p,α)^{14}N reaction rate at temperatures between 10 and 100 MK[3], i.e., over the entire range of interest here. The experiment took place at the Laboratory for Underground Nuclear Astrophysics (LUNA) at Gran

Sasso, Italy, where a 15 times lower background for α particles detection than in surface laboratories allowed for the most sensitive measurement to date[3]. The new rate is 2–2.5 times higher than previous evaluations[8,15]. At the temperatures of 40–55 MK typical of CBP the new rate produces $^{17}O/^{16}O$ values too low to match those observed in Group II grains (Figure 2). At the temperatures of 60–80 MK typical of HBB, instead, the new rate reproduces the observed $^{17}O/^{16}O$ values, revealing these grains as the missing stardust showing the signature expected from HBB in massive AGB stars.

Although the initial stellar mass and metallicity ranges at which HBB occurs as well as the AGB lifetime are model dependent[6,16,17], our result is robust because any massive AGB model experiencing HBB with temperatures between 60 and 80 MK will necesserily result in $^{17}O/^{16}O$ ratios in agreement with those observed in Group II grains. Figure 3 shows the surface evolution of O isotopic ratios for three AGB models (of initial mass 4.5, 5, and 6 $\mathrm{M}_{\odot}$) of solar metallicity that experience HBB (see Methods section), compared to observed isotopic ratios in Group II stardust grains. The models evolve through the first and second dredge-ups at the end of core H- and He-burning, respectively, which increase the $^{17}O/^{16}O$ ratio by roughly a factor of five. During the subsequent AGB phase, HBB quickly (e.g., for the 6 $\mathrm{M}_{\odot}$ model, after the star has evolved through roughly 1/5 of its total AGB lifetime) shifts the O isotopic composition to the equilibrium values at the corresponding burning temperature. Using the LUNA rate, the $^{17}O/^{16}O$ ratio produced by HBB is roughly a factor of two lower than that obtained with the previous rate by Iliadis[8] and nicely replicates measured values in Group II grains, when assuming various degrees of dilution of AGB matter with matter of solar composition. The HBB strongly depletes ^{18}O, which is consistent

with the non-detection of ^{18}O in bright O-rich AGB stars[18], and results in ^{18}O/^{16}O ratios more than two orders of magnitude lower than measured in the Group II grains. Interestingly, the mixing with solar material has a particularly noticeable effect on the ^{18}O/^{16}O ratio. For example, 99% of HBB matter mixed with only 1% of solar material increases the ^{18}O/^{16}O by two orders of magnitudes. Although percent-level traces of contaminant oxygen (e.g., from terrestrial or non-presolar material) during isotopic measurements can result in ^{18}O/^{16}O up to $\sim 10^{-4}$, laboratory contamination cannot easily explain grains with higher ^{18}O/^{16}O values. For these, a dilution of the HBB signature composition with solar system matter at the level of a few tens of percent is required. A possible physical mechanism may involve binary interactions with a lower mass companion. This suggestion is in agreement with the observational evidence that the frequency of multiple systems is $\geq 50\%$ for stars in the mass range considered here[19].

Other isotopic pairs measured in Group II grains are also consistent with an origin in massive AGB stars. The ^{25}Mg/^{24}Mg ratios are enhanced in massive AGB stars by the third dredge-up of matter from the He inter-shell, where the ^{22}Ne(α,n)^{25}Mg reaction is activated, and such a signature is seen in some presolar spinel ($MgAl_2O_4$) grains (top panel of Figure 4). Specifically, the ^{25}Mg/^{24}Mg value observed for a spinel grain named 14-12-7[20] is close to that obtained in the final composition of the 5 $M_\odot$ model, assuming roughly 5% contamination of solar matter. Similarly, grain OC2[10] and some other grains also show excesses in ^{25}Mg, although not as high as the final composition of the predicted evolution plotted in Figure 4. These values can be explained by a less efficient third dredge-up than calculated in our models and/or by a shorter AGB phase (e.g., halved as illustrated in Figures 4 and 3) as a result of a higher mass-loss rate and/or the effect of

binary interactions. Finally, the high ^{26}Al/^{27}Al ratios up to $\sim$0.1 typical of Group II grains are also consistent with HBB (bottom panel of Figure 4), although an accurate analysis is currently hampered by the uncertainties in the proton capture rates of ^{25}Mg[21] and ^{26}Al[8].

We conclude that a fraction of meteoritic stardust grains exist whose O, Mg, and Al isotopic composition is best accounted for by H-burning conditions characteristic of massive AGB stars, when using an improved determination of the ^{17}O(p,α)^{14}N reaction rate. Percentage-level dilution of AGB ejecta with matter of solar composition is required to reproduce a large fraction of the data, suggesting binary interactions during the lives of the parent stars.

Acknowledgements We thank Onno Pols and Rob Izzard for discussion on the frequency of multiple systems in relation to massive AGB stars. ML is a Momentum ("Lendület-2014" Programme) project leader of the Hungarian Academy of Sciences. ML and AIK are grateful for the support of the NCI National Facility at the ANU.

Competing Interests The authors declare that they have no competing financial interests.

Correspondence Correspondence and requests for materials should be addressed to M. Lugaro (email: maria.lugaro@csfk.mta.hu).

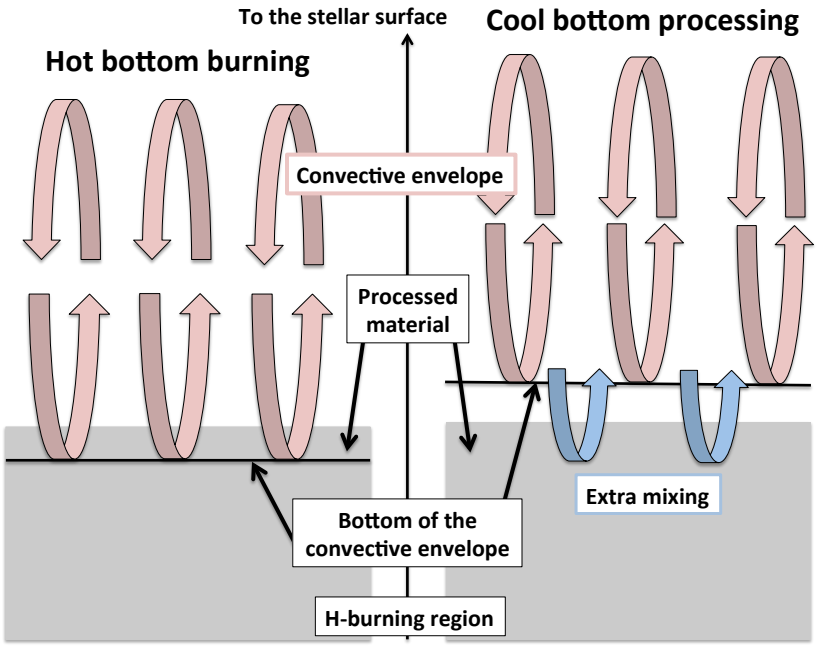

Figure 1: Schematic diagram of the internal structure of AGB stars at the interface between the H-burning region and the convective envelope. Hot bottom burning (HBB, left panel) and cool bottom processing (CBP, right panel) take place in massive and low-mass AGB stars, respectively, and mix to stellar surface material processed in the H-burning region. The main differences between the two cases are that: (1) material is processes at higher temperatures but lower densities in the case of HBB, with respect to CBP; and (2) mixing occur via convection in the case of HBB, while in the case of CBP non-convective extra mixing needs to be invoked.

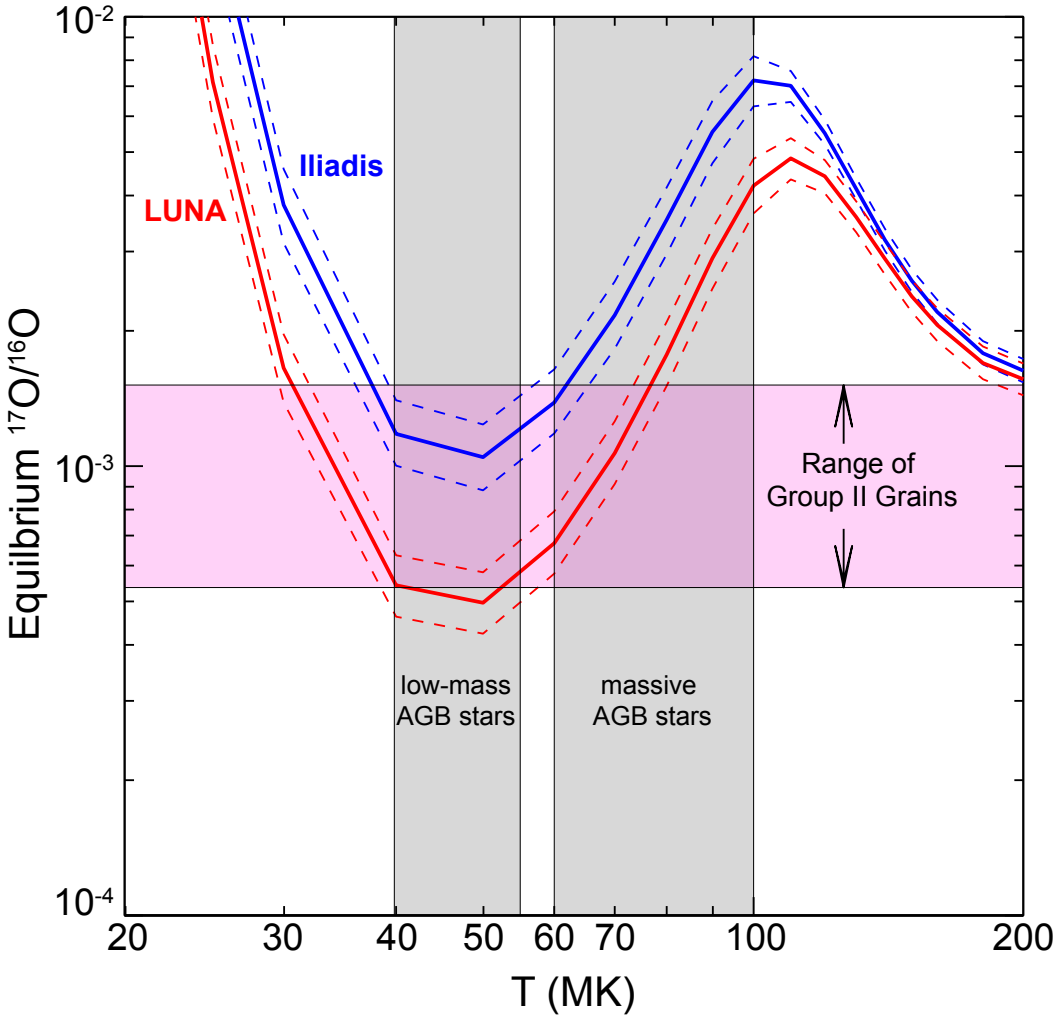

Figure 2: Equilibrium $^{17}O/^{16}O$ ratio defined as the ratio of the production to destruction rates of ^{17}O in the temperature range of interest for AGB stars using the recommended (thick lines) and the lower and upper limits (thin lines) of the $^{17}O(p,\alpha)^{14}N$ reaction rate from LUNA[3] and Iliadis et al.[8]. The horizontal pink band shows the range of $^{17}O/^{16}O$ values observed in Group II grains. The typical temperature ranges for CBP in low-mass AGB stars and for HBB in massive AGB stars are shown as grey vertical bands.

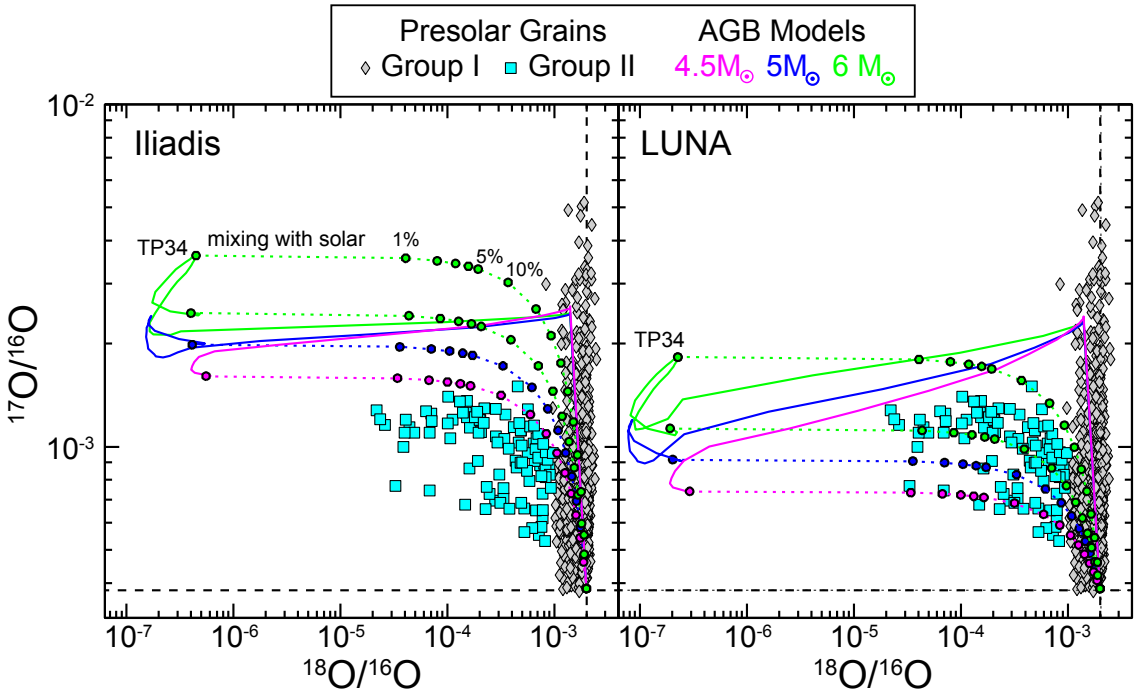

Figure 3: Evolution of the O isotopic ratios calculated at the surface of models of massive AGB stars of solar metallicity as compared to data from Group I and II stardust oxide grains (from the presolar database[22], error bars are omitted for clarity and are within or extremely close to the symbol). Horizontal and vertical dashed black lines represent the solar isotopic values. The models are calculated with the old (Iliadis[8], left panel) and the new (LUNA[3], right panel) ^{17}O(p,α)^{14}N reaction rate. The dotted lines represent an example of the compositions resulting from mixing solar composition material to the AGB composition, taking as illustrative cases the composition at end of the AGB evolution and the composition after the roughly half the AGB timelife for the 6 $M_{\odot}$ star (label TP34, indicates that the star has evolved through 34 out of the total 53 computed thermal instabilities of the He-burning shell). The small circles on top of the dotted lines represent various degrees of % mixing of solar matter.

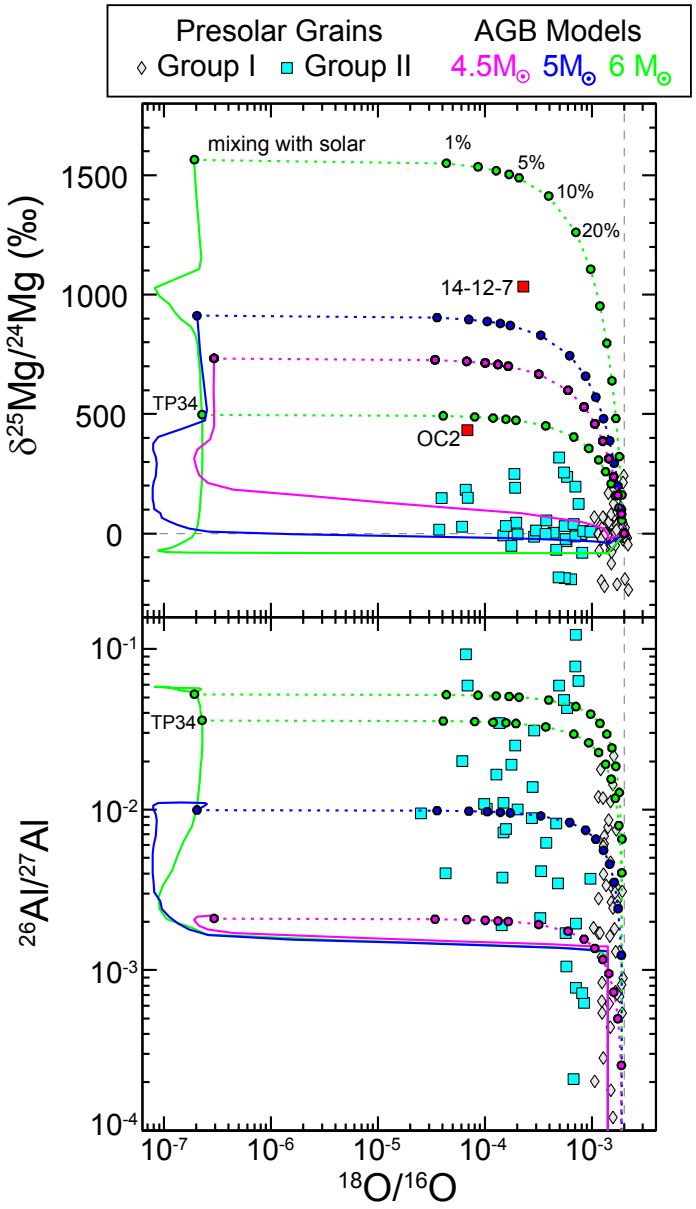

Figure 4: Same as Figure 3 but showing selected O, Mg, and Al isotopic ratios and the models calculated with the LUNA rate. δ^{25}Mg/^{24}Mg-values represent permil variations with respect to the solar system value. The two spinel grains with excesses in ^{25}Mg (OC2 and 14-12-7) are highlighted in red.

Methods

Stellar models

Stellar structure models with metallicities (Z) from half to double solar (where solar is 0.014[25]) were selected from the large set presented by Karakas[24] and computed with the Monash-Stromlo code[23]. No mass-loss was assumed on the red giant branch and the Vassiliadis & Wood[26] mass-loss formulation was used on the AGB. The C-rich and N-rich low-temperature opacity tables were taken from Marigo & Aringer[27]. Convection was approximated using the Mixing-length Theory with a mixing-length parameter of 1.86 in all calculations. No convective overshoot was applied, although the algorithm described by Lattanzio[28] was used to search for a neutrally stable point for the border between convective and radiative zones.

From the models presented by Karakas[24], in the Extended Data Table 1 we present a selection of models with initial masses from 4.5 to 8 $\mathrm{M}_{\odot}$ with canonical values of the He content. More details on the physical quantities of the models can be found in Table 1 of Karakas[24]. Here, we only report a summary of those that are most relevant: the total number of thermal instabilities of the He-burning shell (thermal pulses, TPs); the maximum temperature at the base of the convective envelope ($\mathrm{T}_{\mathrm{bce}}^{\mathrm{max}}$); the maximum temperature achieved in the intershell ($\mathrm{T}_{\mathrm{intershell}}^{\mathrm{max}}$); and the mass lost during the whole evolution ($\mathrm{M}_{\mathrm{lost}}^{\mathrm{total}}$). All the models experienced $\mathrm{T}_{\mathrm{bce}}^{\mathrm{max}}$ high enough to activate HBB, except for the 5 $\mathrm{M}_{\odot}$ model of Z$= 0.03$. It should be noted that the mass and metallicity ranges at which HBB occurs are model dependent. For the same mass and metallicity, models using more or less efficient convection, for example, via a different mixing length parameter or

different mixing schemes, result in different temperatures[6,16]. All our stellar models also experienced efficient third dredge-up, i.e., C-rich material being carried from the He-rich inter-shell to the convective envelope. This is also model dependent. However, because of both the large dilution and the effect of HBB, most of the models lead to O-rich surfaces – the condition for the formation of oxide and silicate grains of interest here – during their whole evolution, except for the 4.5 $\mathrm{M}_{\odot}$ model of Z=0.014 and the 5 $\mathrm{M}_{\odot}$ model of Z=0.007. These latter become C-rich after the second last TP and the last TP, respectively, which results in 40–50% of the material ejected to be C-rich. For all the models, a relatively large fraction of the envelope material (20–30%) is still present when our calculations stopped converging, and is lost carrying the signature of the last computed model.

We fed the computed stellar structure into the Monash post-processing code to calculate the detailed nucleosynthesis by solving simultaneously the abundance changes wrought by nuclear reactions and by convection using a a"donor cell" advective scheme with two-streams (up and down) mixing. The simultaneous treatment of mixing and burning is required to model HBB in detail because nuclear reactions occur that may have timescales similar or shorter than the mixing timescales, also as function of the location in the envelope. In this cases it is not possible to make the assumption of istantaneous mixing at an average burning rate. Essentially our method couples mixing and burning together in the post processing to obtain the nucleosynthesis, while the energetic feedback of HBB is taken from the structure calculations performed using instantaneous mixing. The nucleosynthesis of elements up to Pb and Bi from the complete set of the models of Karakas[24] with He canonical abundance can be found in Karakas & Lugaro[17], together with a

full discussion of the results. Briefly, in models that experience HBB, $\mathrm{T}_{\mathrm{bce}}^{\mathrm{max}}$ is the main feature controlling the composition of the stellar surface, and specifically the O and Al ratios that are measured in oxide and silicate stardust grains. In massive AGB stars of metallicity around solar the Mg composition is affected mainly by the activation of the ^{22}Ne(α,n)^{25}Mg and ^{22}Ne(α,γ)^{26}Mg reactions in the He-rich inter-shell, where $\mathrm{T}_{\mathrm{intershell}}^{\mathrm{max}}$ is well above the activation temperature (T ≈ 300 MK) of these reactions in all the models, and the subsequent third dredge-up of this material to the stellar surface. With respect to Karakas & Lugaro[17], we updated the ^{22}Ne+α reaction rates from Iliadis et al.[8] to Longland et al.[29] and the ^{25}Mg+γ reaction rates from Iliadis et al.[8] to Straniero et al.[21]. Also, in the present study, we limited our calculations to a small network of 77 nuclear species, from neutrons to sulfur, plus elements around the Fe peak, as described, *e.g.*, in Karakas[23]. This choice allowed us to run each model in a few hours and test different values of the ^{17}O(p,α)^{14}N reaction rate: the recommended, the upper limit, and the lower limit from both Iliadis et al.[8] and LUNA[3]. For the ^{16}O(p,γ)^{17}F rate we used the value recommended by Iliadis et al.[8], which has an uncertainty of 7%[11]. For the initial composition, we used Asplund et al.[25] for the solar metallicity models, scaled down or up by factor of two for the Z=0.007 and Z=0.03 models, respectively. While we run detailed model predictions for all the models listed in the Extended Data Table 1, in the figures and discussion we focus on the 4.5, 5, and 6 $\mathrm{M}_{\odot}$ models with Z=0.014 only, for the sake of clarity. Models with different metallicities in the same mass range have similar $\mathrm{T}_{\mathrm{bce}}^{\mathrm{max}}$ and provide similar results. On the other hand, our 8 $\mathrm{M}_{\odot}$ models have too high $\mathrm{T}_{\mathrm{bce}}^{\mathrm{max}}$ to provide a match with the grain data (see Figure 2).

1. Gail, H.-P., Zhukovska, S. V., Hoppe, P. & Trieloff, M. Stardust from Asymptotic Giant

Branch Stars. *Astrophys. J.* **698**, 1136–1154 (2009).

2. Zhukovska, S., Petrov, M. & Henning, T. Can Star Cluster Environment Affect Dust Input From Massive AGB Stars? *Astrophys. J.* **810**, 128 (2015). 1508.01035.

3. Bruno, C. Accurate direct measurement of the 70 keV resonance strength in the ^{17}O(p,α)^{14}N reaction at LUNA. *Phys. Rev. Lett.* (2016).

4. Zinner, E. Presolar Grains. In Davis, A. M. (ed.) *Microphysics of Cosmic Plasmas*, 181–213 (2014).

5. Nittler, L. R., Alexander, C. M. O., Gao, X., Walker, R. M. & Zinner, E. Stellar Sapphires: The Properties and Origins of Presolar AL 2O 3 in Meteorites. *Astrophys. J.* **483**, 475 (1997).

6. Ventura, P., Di Criscienzo, M., Carini, R. & D'Antona, F. Yields of AGB and SAGB models with chemistry of low- and high-metallicity globular clusters. *Mon. Not. R. Astron. Soc.* **431**, 3642–3653 (2013).

7. Wood, P. R., Bessell, M. S. & Fox, M. W. Long-period variables in the Magellanic Clouds - Supergiants, AGB stars, supernova precursors, planetary nebula precursors, and enrichment of the interstellar medium. *Astrophys. J.* **272**, 99–115 (1983).

8. Iliadis, C., Longland, R., Champagne, A. E., Coc, A. & Fitzgerald, R. Charged-particle thermonuclear reaction rates: II. Tables and graphs of reaction rates and probability density functions. *Nuclear Physics A* **841**, 31–250 (2010).

9. Boothroyd, A. I., Sackmann, I.-J. & Wasserburg, G. J. Hot bottom burning in asymptotic giant branch stars and its effect on oxygen isotopic abundances. *Astrophys. J. Lett.* **442**, L21–L24 (1995).

10. Lugaro, M. *et al.* On the asymptotic giant branch star origin of peculiar spinel grain OC2. *Astron. Astrophys.* **461**, 657–664 (2007). astro-ph/0610464.

11. Iliadis, C., Angulo, C., Descouvemont, P., Lugaro, M. & Mohr, P. New reaction rate for O16(p,γ)F17 and its influence on the oxygen isotopic ratios in massive AGB stars. *Phys. Rev. C* **77**, 045802 (2008). 0803.2757.

12. Nollett, K. M., Busso, M. & Wasserburg, G. J. Cool Bottom Processes on the Thermally Pulsing Asymptotic Giant Branch and the Isotopic Composition of Circumstellar Dust Grains. *Astrophys. J.* **582**, 1036–1058 (2003).

13. Palmerini, S., La Cognata, M., Cristallo, S. & Busso, M. Deep Mixing in Evolved Stars. I. The Effect of Reaction Rate Revisions from C to Al. *Astrophys. J.* **729**, 3 (2011).

14. Nucci, M. C. & Busso, M. Magnetohydrodynamics and Deep Mixing in Evolved Stars. I. Two- and Three-dimensional Analytical Models for the Asymptotic Giant Branch. *Astrophys. J.* **787**, 141 (2014). 1404.2503.

15. Buckner, M. Q. *et al.* High-intensity-beam study of ^{17}O(p ,γ)^{18}F and thermonuclear reaction rates for ^{17}O+p. *Phys. Rev. C* **91**, 015812 (2015).

16. Cristallo, S., Straniero, O., Piersanti, L. & Gobrecht, D. Evolution, Nucleosynthesis, and Yields of AGB Stars at Different Metallicities. III. Intermediate-mass Models, Revised Low-mass Models, and the ph-FRUITY Interface. *Astrophys. J. Suppl.* **219**, 40 (2015).

17. Karakas, A. I. & Lugaro, M. Stellar yields from metal-rich asymptotic giant branch models. *Astrophys. J.* (2016).

18. Justtanont, K. *et al.* Herschel observations of extreme OH/IR stars. The isotopic ratios of oxygen as a sign-post for the stellar mass. *Astron. Astrophys.* **578**, A115 (2015).

19. Duchêne, G. & Kraus, A. Stellar Multiplicity. *Ann. Rev. Astron. Astrophys.* **51**, 269–310 (2013). 1303.3028.

20. Gyngard, F. *et al.* Automated NanoSIMS Measurements of Spinel Stardust from the Murray Meteorite. *Astrophys. J.* **717**, 107–120 (2010). 1006.4355.

21. Straniero, O. *et al.* Impact of a Revised ^{25}Mg(p, γ)^{26}Al Reaction Rate on the Operation of the Mg-Al Cycle. *Astrophys. J.* **763**, 100 (2013).

22. Hynes, K. M. & Gyngard, F. The Presolar Grain Database: http://presolar.wustl.edu/˜pgd. In *Lunar and Planetary Science Conference*, vol. 40 of *Lunar and Planetary Science Conference*, 1198 (2009).

23. Karakas, A. I. Updated stellar yields from asymptotic giant branch models. *Mon. Not. R. Astron. Soc.* **403**, 1413–1425 (2010).

24. Karakas, A. I. Helium enrichment and carbon-star production in metal-rich populations. *Mon. Not. R. Astron. Soc.* **445**, 347–358 (2014).

25. Asplund, M., Grevesse, N., Sauval, A. J. & Scott, P. The Chemical Composition of the Sun. *Ann. Rev. Astron. Astrophys.* **47**, 481–522 (2009).

26. Vassiliadis, E. & Wood, P. R. Evolution of low- and intermediate-mass stars to the end of the asymptotic giant branch with mass loss. *Astrophys. J.* **413**, 641–657 (1993).

27. Marigo, P. & Aringer, B. Low-temperature gas opacity. ÆSOPUS: a versatile and quick computational tool. *Astron. Astrophys.* **508**, 1539–1569 (2009).

28. Lattanzio, J. C. The asymptotic giant branch evolution of 1.0-3.0 solar mass stars as a function of mass and composition. *Astrophys. J.* **311**, 708–730 (1986).

29. Longland, R., Iliadis, C. & Karakas, A. I. Reaction rates for the s-process neutron source ^{22}Ne + α. *Phys. Rev. C* **85**, 065809 (2012).